

# Local post-processing for locally conservative fluxes in the Galerkin method for groundwater flows

E. T. Coon,<sup>1</sup> S. P. MacLachlan,<sup>2</sup> and J. D. Moulton,<sup>3</sup>

**Abstract.** The Galerkin Finite-Element Method using bilinear basis functions (in two dimensions) offers many advantages in the numerical treatment of flow through porous media. A significant disadvantage of this approach, however, is the lack of an explicit discrete requirement of conservation of mass on mesh cells. While this shortcoming is a concern in the case of single-phase flows, it is critical in the case of multi-phase flows, where lack of conservation may lead to inaccurate or non-physical simulations. Here, we extend the approach of *Cordes and Kinzelbach* [1992] for computing continuous velocity fields based on finite-element solution data to the important cases of heterogeneous media, non-zero recharge, and non-homogeneous boundary conditions. We introduce a new technique, which solves a problem similar to that in *Cordes and Kinzelbach* [1992], but using a local mixed finite element basis. Finally, we compare the two approaches and give numerical results that demonstrate the usefulness of the improved velocity fields.

## 1. Introduction

The continuous Galerkin Finite Element Method (hereafter GFEM) has many advantages for the numerical modeling of flow through porous media. One advantage is the properties of the resulting discrete matrix equations, which are optimally solved using methods such as multigrid (*Ruge and Stüben* [1987]; *Dendy* [1982]; *Alcouffe et al.* [1981]). This method solves the second-order form of porous flow for pressure, while fluxes must be calculated via post-processing. The simplest post-processing applies Darcy's Law directly to the pressure solution, but this results in a locally non-conservative flow field.

Although the necessity of conservative fluxes for single-phase flow is unclear (see, e.g., the discussion in *Mosé et al.* [1994]), it is essential for applications such as multi-phase flow or reactive transport, where non-conservative fluxes can generate negative concentrations and other non-physical results. Therefore, many researchers have turned to the first-order form of the flow equations, because such approaches explicitly build local mass conservation into the discretization. These discretizations include Finite Volumes, Mixed Finite Elements, and Discontinuous Galerkin methods, among others. However, due to the additional complexity of these discretization methods, the appeal of the GFEM remains. Moreover, the GFEM *does* have a discrete mass conservation statement in its equations. This statement is a weak condition with no explicit control volume (*Cordes and Kinzelbach* [1996]; *Hughes et al.* [2000]); however, it can still be used to derive various projections and post-processing techniques. For example, *Wheeler* [1974] presented a one-dimensional post-processing technique that results in superconverging fluxes at nodes. *Carey et al.* [1985] extended this to two dimensions, resulting in methods for developing globally conservative fluxes. More recent efforts, including *Hughes et al.* [2000], *Carey* [2002], and *Cockburn et al.*

[2007], have generated various methods to post-process for locally conservative fluxes.

All of these methods define global post-processing problems; a linear system on the entire domain must be solved. In many simulations where multiscale or upscaling algorithms are used (cf. *MacLachlan and Moulton* [2006]; *Hou and Wu* [1997]; *Hou et al.* [1999]; *Arbogast* [2000]; *Efendiev and Durlofsky* [2002]; *Hughes et al.* [1998]), global solves on the finest scale, whether for pressure or post-processing of fluxes, are not computationally feasible. Indeed, even in the case where global pressure solves are feasible, the cost of global post-processing for locally conservative fluxes may be prohibitive. To retain the efficiency of computation with upscaled pressure fields, the calculation of fluxes must not use global solves.

Alternatively, *Cordes and Kinzelbach* [1992] presented an algorithm in which the weak conservation statement in GFEM is enforced on a specified control volume. In this method, a series of local problems are solved for edge fluxes that are locally conservative by construction. This approach requires no global solves, so the method works well for multiscale applications.

In the method of *Cordes and Kinzelbach*, a refined dual mesh is introduced and local mass balance equations are defined on dual mesh cells. These equations are closed through an irrotationality constraint. In Section 2, we review and extend this method, allowing for anisotropic and heterogeneous permeability, nonzero source terms, and nontrivial boundary conditions. In Section 3, we introduce a new approach, where mixed finite elements are used to discretize local problems on the same dual mesh. This leads to the same local mass balance equations, but with a new closure. We provide numerical examples in Section 4 that demonstrate the superconvergence of the resulting fluxes, and compare the accuracy of the two approaches. Finally, we apply the method to a physically relevant permeability field.

## 2. Generalization of the Cordes and Kinzelbach Method

Saturated flow in porous media is governed by two equations: mass balance

$$\nabla \cdot \mathbf{v} = f, \quad (1)$$

and Darcy's law,

$$\mathbf{v} = -\kappa \nabla p. \quad (2)$$

<sup>1</sup>Applied Physics and Applied Mathematics, Columbia University, New York, NY 10027 USA.

<sup>2</sup>Department of Mathematics, Tufts University, Medford, MA 02155, USA.

<sup>3</sup>Applied Mathematics and Plasma Physics, Los Alamos National Laboratory, Los Alamos, NM 87545, USA

The former balances the flow field  $\mathbf{v}$  with source terms  $f$ . The latter defines velocity  $\mathbf{v}$  throughout the domain as a function of pressure  $p$  and permeability  $\mathcal{K}$ . Together, these equations are called the first-order form. The second-order form combines these equations into a single, elliptic equation for pressure,

$$-\nabla \cdot \mathcal{K} \nabla p = f. \quad (3)$$

Here, we consider a rectangular domain,  $\Omega \subset \mathbb{R}^2$ , with a Cartesian mesh. We use the GFEM with bilinear basis functions for pressure to discretize (3). Appropriate boundary conditions are specified, and the resulting discrete system is solved using multigrid. The solution of weights,  $\mathbf{p}_i$ , where  $p \equiv \sum_i \mathbf{p}_i \phi_i$ , are taken as input data to post-process.

In our discrete equations, we need to index elements that surround a given node, nodes that border a given element, and other topological relations. Indices  $i$  and  $j$  are used to index nodes,  $e$  is used to index elements, and  $s$  is used to index side edges of the elements. On this quadrilateral mesh, we introduce the sets  $\mathcal{C} \equiv \{N, S, E, W\}$  and  $\mathcal{D} \equiv \{NW, NE, SW, SE\}$ , to index topological relations between nodes, edges, and quadrilateral elements. Furthermore, subscripts indicate the base object to which the superscripted index is referring. For instance,  $q_i^s$  for each  $s \in \mathcal{C}$  refers to the fluxes along the edges to the North, South, East, and West of node  $i$ , while  $\Omega_i^e$  for each  $e \in \mathcal{D}$  indexes the elements to the Northwest, Northeast, Southwest, and Southeast of node  $i$ .

Under the GFEM, the weak form of (1) near node  $i$  is given by:

$$\sum_{e \in \mathcal{D}} \int_{\Omega_i^e} \phi_i \nabla \cdot \mathbf{v} = \sum_{e \in \mathcal{D}} \int_{\Omega_i^e} \phi_i f. \quad (4)$$

Noting that the basis function,  $\phi_i$ , is zero on the outer boundary of the patch defined by  $\Omega_i^e$  for all  $e \in \mathcal{D}$ , the divergence theorem and product rule yield

$$-\sum_{e \in \mathcal{D}} \int_{\Omega_i^e} \nabla \phi_i \cdot \mathbf{v} = \sum_{e \in \mathcal{D}} \int_{\Omega_i^e} \phi_i f. \quad (5)$$

A weak, nodal flux,  $Q_i^e$ , from node  $i$  to each neighboring element  $\Omega_i^e$  and local source terms,  $F_i^e$ , can then be defined as

$$Q_i^e \equiv - \int_{\Omega_i^e} \nabla \phi_i \cdot \mathbf{v} \quad \text{and} \quad F_i^e \equiv \int_{\Omega_i^e} \phi_i f, \quad (6)$$

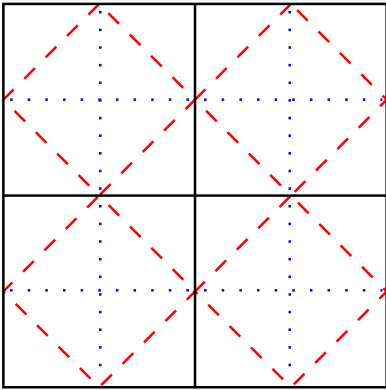


**Figure 1.** Dual mesh on which conservation principles are enforced. For this and all figures, solid black lines are the grid lines of the original Cartesian mesh, dotted blue lines are the refined mesh on which we will define unknown fluxes  $q$ , and dashed red lines are the dual mesh on which nodal fluxes  $Q$  are assumed to exist. Control volumes for conservation equation (7) consist of these dual-cell diamonds.

respectively, resulting in a discrete mass-conservation equation,

$$\sum_{e \in \mathcal{D}} Q_i^e = \sum_{e \in \mathcal{D}} F_i^e. \quad (7)$$

These nodal fluxes are evaluated from the local bilinear pressure solution given on each element and Equation (2):

$$\begin{aligned} Q_i^e &= \int_{\Omega_i^e} \nabla \phi_i \cdot (\mathcal{K}_i^e \nabla p) \\ &= \int_{\Omega_i^e} \nabla \phi_i \cdot \left( \mathcal{K}_i^e \nabla \left( \sum_{j \in \mathcal{D}} \mathbf{p}_e^j \phi_e^j \right) \right), \end{aligned} \quad (8)$$

where the  $\mathbf{p}_e^j$  refer to pressures at the nodes  $j \in \mathcal{D}$  around element  $e$  and the  $\phi_e^j$  are the nodal basis functions. While mass conservation is not explicitly included in this second-order form of the GFEM discretization, this weak mass-conservation principle is enforced. However, as both  $\mathbf{v}$  and  $\phi_i$  vary throughout element  $e$ , this conservation equation does not have an explicit control volume associated with it. To define a control volume, a refined dual mesh is formed by connecting midpoints of the Cartesian mesh edges. The nodal fluxes  $Q_i^e$  are taken to be the averaged flux across dual cell edges, as shown in Figure 1.

This dual mesh gives rise to three types of local control volumes: those centered on nodes, those entirely contained within elements, and incomplete dual cells that intersect the boundary of  $\Omega$ . Using the  $Q_i^e$  as boundary data on these

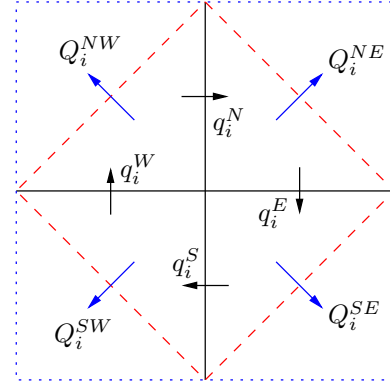


**Figure 2.** Local problem domain around node  $i$ . Fluxes from node  $i$  to elements  $e \in \mathcal{D}$ ,  $Q_i^e$ , are specified as boundary data for the local problem, while refined fluxes around node  $i$ ,  $q_i^s$ , for edges  $s \in \mathcal{C}$ , are unknowns to be determined.

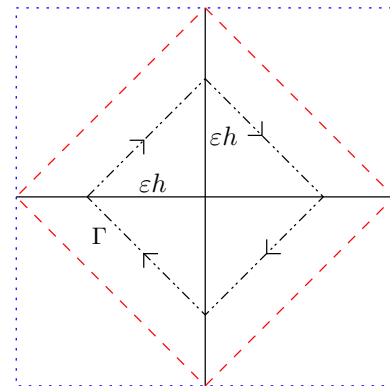


**Figure 3.** Path taken for integration of irrotationality constraint around a typical interior cell.

dual cells, we calculate the interior refined fluxes,  $\{q_i^s\}_{s \in \mathcal{C}}$ , defined as fluxes on half-edges of the original GFEM mesh.

For the sake of simplicity, we assume throughout the following that the Cartesian mesh is uniform with square elements of size  $h$ . This is not a limitation of the method; similar results have been derived for non-square meshes. Also, permeability  $\mathcal{K}$  is assumed to be a piecewise constant tensor on the mesh cells, with arbitrary jumps across mesh edges.

### 2.1. Node-Centered Dual Cells

On node-centered dual cells, the local problem domain is shown in Figure 2. Mass balance in each sub-cell of the dual mesh provides the following four discrete equations,

$$\begin{aligned} q_i^W - q_i^N &= Q_i^{NW} - F_i^{NW}, \\ q_i^S - q_i^W &= Q_i^{SW} - F_i^{SW}, \\ q_i^E - q_i^S &= Q_i^{SE} - F_i^{SE}, \\ q_i^N - q_i^E &= Q_i^{NE} - F_i^{NE}. \end{aligned} \quad (9)$$

Summing these equations yields (7), which enforces mass conservation on the entire dual cell. However, as the left-hand sides of these equations sum to zero, only three of the four equations are linearly independent.

To make the system well-posed, the additional constraint of irrotationality around node  $i$  is added. At any point in the domain where  $p$  is sufficiently differentiable,  $\nabla \times \nabla p = 0$  identically, implying that over any closed path  $\Gamma$  contained in  $\Omega$ ,

$$\oint_{\Gamma} \nabla p \cdot ds = 0 \quad (10)$$

by Green's Theorem. This path is chosen to be the dual-cell boundary, shrunk uniformly via a parameter  $\varepsilon$  around node  $i$  (Figure 3). To simplify this, write  $\nabla p = \mathcal{K}^{-1} \mathbf{v}$ , and note that, as  $\varepsilon \rightarrow 0$ ,  $\mathbf{v}$  can be approximated by the (constant) velocities on the edges of the appropriate quadrant. For example,

$$\mathbf{v}^{NW} \approx \frac{2}{h} \begin{bmatrix} q^N \\ q^W \end{bmatrix}. \quad (11)$$

Evaluating Equation (10) over this path then results in a fourth, linearly independent equation for the unknowns  $q_i^s$  for  $s \in \mathcal{C}$ ,

$$a_N q_i^N + a_W q_i^W + a_S q_i^S + a_E q_i^E = 0, \quad (12)$$

where

$$\begin{aligned} a_N &= \{\mathcal{K}_{NE}^{-1}\}_{11} - \{\mathcal{K}_{NE}^{-1}\}_{12} + \{\mathcal{K}_{NW}^{-1}\}_{11} + \{\mathcal{K}_{NW}^{-1}\}_{12}, \\ a_W &= \{\mathcal{K}_{SW}^{-1}\}_{22} - \{\mathcal{K}_{SW}^{-1}\}_{12} + \{\mathcal{K}_{NW}^{-1}\}_{22} + \{\mathcal{K}_{NW}^{-1}\}_{12}, \\ a_S &= \{\mathcal{K}_{SW}^{-1}\}_{11} - \{\mathcal{K}_{SW}^{-1}\}_{12} + \{\mathcal{K}_{SE}^{-1}\}_{11} + \{\mathcal{K}_{SE}^{-1}\}_{12}, \\ a_E &= \{\mathcal{K}_{NE}^{-1}\}_{22} - \{\mathcal{K}_{NE}^{-1}\}_{12} + \{\mathcal{K}_{SE}^{-1}\}_{22} + \{\mathcal{K}_{SE}^{-1}\}_{12}. \end{aligned}$$

Three mass balance equations from (9) and this irrotationality constraint (12), are solved for the refined fluxes.

### 2.2. Element-Centered Dual Cells

Element-centered dual cells are handled similarly to node-centered cells. The local problem domain is shown in Figure 4. As all sources are handled in the node-based dual cells, local mass balance implies

$$\begin{aligned} q_e^W - q_e^N &= -Q_e^{NW}, \\ q_e^S - q_e^W &= -Q_e^{SW}, \\ q_e^E - q_e^S &= -Q_e^{SE}, \\ q_e^N - q_e^E &= -Q_e^{NE}, \end{aligned} \quad (13)$$

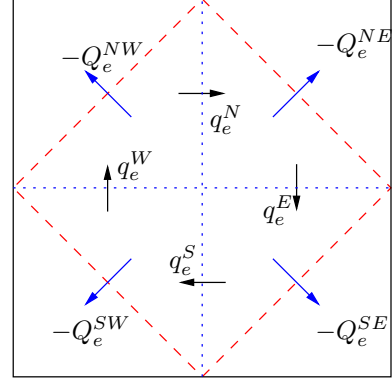


**Figure 4.** Local problem domain within an element. Fluxes are the negative of the corresponding nodal fluxes.

where the fluxes from the nodes,  $j \in \mathcal{D}$ , to element  $e$ , given by  $Q_e^j$ , are negated to match the outward flux convention. As before, these equations are linearly dependent, and irrotationality is used to close the system. Since, in this case, the permeability is constant throughout the cell, velocities are continuous along the corresponding path  $\Gamma$  (now centered at the center of element  $e$ ). The corresponding irrotationality constraint is given by

$$\{\mathcal{K}_e^{-1}\}_{11} (q_e^N + q_e^S) + \{\mathcal{K}_e^{-1}\}_{22} (q_e^E + q_e^W) = 0. \quad (14)$$

Three mass balance equations from (13) and this irrotationality constraint (3), are solved for the refined fluxes.

### 2.3. Dual Cells Adjacent to the Boundary

On a Cartesian mesh, all dual cells that intersect the domain boundary are located at nodes and consist of either edges or corners. In edge cases, dual cells consist of three unknown fluxes, and two mass-balance equations. See, for example, Figure 5. In corner cases, dual cells consist of two unknown fluxes and one mass-balance equation.

Global boundary conditions must now be applied. In the case of one or more edges with Neumann data, these

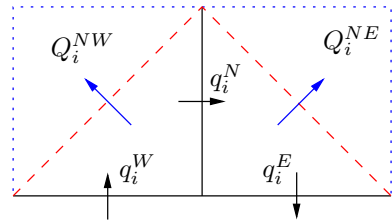


**Figure 5.** Local problem domain at an edge. In the case of Neumann boundary conditions,  $q_i^W$  and  $q_i^E$  are known, while, for Dirichlet data, they must be determined.

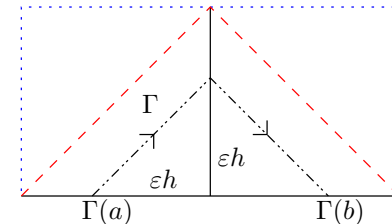


**Figure 6.** Path taken for integration of rotationality constraint in a boundary cell.

edge fluxes are fixed by the Neumann data. Discrete mass-balance equations completely determine (or potentially over-determine) the system.

In the case of Dirichlet pressure boundary data everywhere, the pressure field has incorporated this data already. Thus, while the mass-balance equations are not singular, the system is still under-determined. The system is again closed via irrotationality. However, no closed path around node  $i$  can be completely contained in  $\Omega$ . Instead, we consider the full form of (10) for a path,  $\Gamma$ , parametrized as  $\mathbf{x}(s)$  for  $s \in [a, b]$ ,

$$\int_{\Gamma} \nabla p \cdot ds = p(\mathbf{x}(b)) - p(\mathbf{x}(a)), \quad (15)$$

by the Fundamental Theorem of Calculus for line integrals. Again, this path is taken to be the dual-cell edges, shrunk uniformly to the node  $i$ , as in Figure 6. For a bilinear pressure field, the pressure difference on the right-hand side of (15) is given by a scaled difference between pressures at the neighboring nodes, for example in the case of Figure 5,

$$p(\mathbf{x}(b)) - p(\mathbf{x}(a)) = \varepsilon (\mathbf{p}_{i+1} - \mathbf{p}_{i-1}). \quad (16)$$

For example, in the case of a node on the bottom boundary, the full irrotationality equation is given as

$$a_E q_i^E + a_N q_i^N + a_W q_i^W = \frac{(\mathbf{p}_{i+1} - \mathbf{p}_{i-1})}{2}, \quad (17)$$

where

$$\begin{aligned} a_E &= \{\mathcal{K}_{NE}^{-1}\}_{22} - \{\mathcal{K}_{NE}^{-1}\}_{12}, \\ a_N &= \{\mathcal{K}_{NE}^{-1}\}_{11} - \{\mathcal{K}_{NE}^{-1}\}_{12} + \{\mathcal{K}_{NW}^{-1}\}_{11} + \{\mathcal{K}_{NW}^{-1}\}_{12}, \\ a_W &= \{\mathcal{K}_{NW}^{-1}\}_{22} + \{\mathcal{K}_{NW}^{-1}\}_{12}. \end{aligned}$$

## 2.4. Aggregation

Once the refined fluxes,  $q_i^s$  and  $q_e^s$  for  $s \in \mathcal{C}$ , are calculated, they are aggregated to form fluxes on centers of the original Cartesian mesh edges, in the same locations that fluxes in mixed FEM or Finite Volume methods would be specified. This is done by simply summing two fluxes on the refined mesh to determine fluxes on the original mesh. Equivalently, velocities are aggregated by averaging the velocity on the two segments. This aggregation process eliminates dependence on the cell-centered dual cell fluxes. As will be demonstrated via numerical experiment in Section 4, this aggregation recovers superconvergence on centers of edges of the original, unrefined mesh.

## 3. Local Boundary Value Problems

Second-order-form methods like GFEM result in discontinuous, non-conservative fluxes when the fluxes are determined directly from (2) using piecewise bilinear pressure basis functions. In the previous section, a discrete mass balance equation satisfied by discrete fluxes was derived. Once an appropriate control volume is associated with this mass balance equation, conservative flux fields were determined.

The method described in Section 2, based on enforcing local irrotationality, is only one approach to determining locally conservative flux fields based on second-order-form pressure data. Here, we consider the same local problems as those in Section 2. However, instead of applying an irrotationality constraint, we now discretize and solve these local problems using standard mixed finite elements to calculate the refined fluxes,  $q_i^s$  and  $q_e^s$ . This method is shown to be equivalent to the previous (geometric) approach in cases without recharge, and the difference between the two methods in the presence of recharge is derived.

### 3.1. Local Problem Method

The local problems on a dual cell, given flux boundary conditions  $Q_i^e$  and sources  $F_i^e$  as defined in (6), are solved using the first-order form. Note that source terms include the integrated source over the entire element from the original mesh, and not just contributions from the dual-mesh element. As a result, element-centered dual cells have no source terms; this is necessary to maintain consistency with the weak conservation law enforced in the pressure solve.

The first-order weak form given by mixed finite elements is

$$\int_{\Omega} \mathbf{u} \cdot (\mathcal{K}^{-1} \mathbf{v}) - \int_{\Omega} (\nabla \cdot \mathbf{u}) p = \int_{\partial\Omega^D} (\nabla \cdot \mathbf{u}) g^D \quad (18)$$

$$\forall \mathbf{u} \in \mathcal{H}(\text{div}; \Omega),$$

$$- \int_{\Omega} (\nabla \cdot \mathbf{v}) w = - \int_{\Omega} f w \quad (19)$$

$$\forall w \in \mathcal{L}^2(\Omega),$$

for Dirichlet pressure boundary data,  $g^D$  on  $\partial\Omega^D$ . The problem is discretized by selecting finite-dimensional subspaces of  $\mathcal{L}^2(\Omega)$  and  $\mathcal{H}(\text{div}; \Omega)$  to approximate  $p$ ,  $w$ ,  $\mathbf{u}$ , and  $\mathbf{v}$ . Using lowest-order Raviart-Thomas mixed finite elements (*Raviart and Thomas [1977]*), the four triangular quadrants of the dual cell are considered elements. Pressure basis functions,  $\varphi$ , are piecewise constant on these elements, and linear flux basis functions are defined by

$$(\psi_{\ell} \cdot \mathbf{n}_m)(\mathbf{x}_m) = \begin{cases} 1, & \text{if } \ell = m \\ 0, & \text{otherwise} \end{cases} \quad (20)$$

where  $\mathbf{x}_m$  is the midpoint of edge  $m$  and  $\mathbf{n}_m$  is the normal vector to edge  $m$ . Because the Raviart-Thomas elements satisfy Equation (20), the discrete representation of (19) is an explicit statement of local mass conservation.

Integration and assembly in these dual cells result in the block matrix equations

$$\begin{bmatrix} \mathbb{A} & \mathbb{B}^T \\ \mathbb{B} & 0 \end{bmatrix} \begin{bmatrix} \mathbf{q}_i \\ \mathbf{p}_i \end{bmatrix} = \begin{bmatrix} 0 \\ -F_i \end{bmatrix}, \quad (21)$$

where entries of  $\mathbb{A}$  and  $\mathbb{B}$  are given by, respectively,

$$a_{\ell m} = \int_{\Omega} \psi_{\ell} \cdot (\mathcal{K}^{-1} \psi_m) \quad \text{and} \quad b_{\ell m} = - \int_{\Omega} \varphi_{\ell} \nabla \cdot \psi_m. \quad (22)$$

Within each block's entries,  $\ell$  and  $m$  refer to a global numbering of the basis functions, where  $\psi$  represents basis functions in  $\mathcal{H}(\text{div}; \Omega)$ , and  $\phi$  represents basis functions in  $\mathcal{L}^2(\Omega)$ . This discrete system of equations uniquely determines the weight vectors  $\mathbf{q}_i$  and  $\mathbf{p}_i$  associated with corresponding basis functions,  $\psi$  and  $\phi$ .

On node-centered interior problems, the unknowns in Equation (21) are four pressure weights,  $\mathbf{p}_i^e$  for  $e \in \mathcal{D}$ , and four interior flux weights,  $q_i^s$  for  $s \in \mathcal{C}$ . Boundary conditions on the local problem are given by specifying the fluxes,  $Q_i^e$ , from Equation (8) across the dual-mesh edges, following the discrete conservation law in Equation (7). Sources on these cells,  $F_i^e$  for  $e \in \mathcal{D}$ , are taken from Equation (6).

This system is solved for the four unknown interior fluxes. To do this, the vector of flux unknowns,  $\mathbf{q}_i$ , is first partitioned into two pieces, the weights,  $q_i^s$  for  $s \in \mathcal{C}$ , of the interior basis functions (corresponding to the fluxes on the edges of the refined mesh) and the weights,  $Q_i^e$  for  $e \in \mathcal{D}$ , of the basis functions on the edges of dual mesh, which are

treated as known using Equation (8). This induces a partitioning on the matrix,  $\mathbb{A}$ , into block two-by-two form,

$$\begin{bmatrix} \mathbb{A}_{11} & \mathbb{A}_{12} & \mathbb{B}_{11}^T \\ \mathbb{A}_{12}^T & \mathbb{A}_{22} & \mathbb{B}_{12}^T \\ \mathbb{B}_{11} & \mathbb{B}_{12} & 0 \end{bmatrix} \begin{bmatrix} q_i \\ Q_i \\ \mathbf{p}_i \end{bmatrix} = \begin{bmatrix} 0 \\ 0 \\ -F_i \end{bmatrix}. \quad (23)$$

Once assembled, the  $\mathbb{B}$  matrices consist of zeros and plus or minus ones, indicating the direction of the contribution of flux basis functions to mass conservation. As the  $\mathbb{B}_{12}$  matrix specifies the flux across a dual-cell edge into the corresponding element,  $\mathbb{B}_{12} = -\mathbb{I}$ .

The  $Q_i^e$  are known via (8), so these are treated as Dirichlet data in the mixed form. Therefore, this block of degrees of freedom can be eliminated, resulting in a reduced system,

$$\begin{bmatrix} \mathbb{A}_{11} & \mathbb{B}_{11}^T \\ \mathbb{B}_{11} & 0 \end{bmatrix} \begin{bmatrix} q_i \\ \mathbf{p}_i \end{bmatrix} = \begin{bmatrix} -\mathbb{A}_{12}Q_i \\ -F_i + Q_i \end{bmatrix}. \quad (24)$$

Solution of this system determines the refined fluxes on node-centered dual cells.

For element-centered dual cells, the problem setup is identical, with element-centered degrees of freedom instead of nodal-centered variables; in this case, the vector of sources,  $F_e$ , is identically zero. For local problems that intersect the boundary of  $\Omega$ , smaller systems are derived and boundary data from the original global problem is applied: Neumann flux data on  $\partial\Omega$  specifies the edge fluxes for the local problem, while Dirichlet pressure data is incorporated directly in the weak form in Equation (18). These problems become simplified versions of the node-centered case and, so, we focus on this case only.

### 3.2. Method Comparison in the Node-Centered Case

To compare the two methods, we manipulate the system above to derive a closure for the mass balance equations. This closure can then be compared to Equation (12). When written out, the second block of equations in (24) is

$$\begin{bmatrix} -1 & 1 & 0 & 0 \\ 0 & -1 & 1 & 0 \\ 0 & 0 & -1 & 1 \\ 1 & 0 & 0 & -1 \end{bmatrix} \begin{bmatrix} q_i^N \\ q_i^W \\ q_i^S \\ q_i^E \end{bmatrix} = \begin{bmatrix} -F_i^{NW} + Q_i^{NW} \\ -F_i^{SW} + Q_i^{SW} \\ -F_i^{SE} + Q_i^{SE} \\ -F_i^{NE} + Q_i^{NE} \end{bmatrix} \quad (25)$$

which is identical to (9). This block is singular, as the boundary-value problem is specified with all-Neumann data; similarly, a constant shift in the pressures,  $\mathbf{p}_i^e$  for  $e \in \mathcal{D}$ , is in the null space of  $\mathbb{B}_{11}^T$ . To account for this, one pressure unknown is fixed. Next, eliminating  $\mathbb{A}_{12}Q_i$  in the upper block of the right-hand side of (24) gives

$$(\mathbb{A}_{11} + \mathbb{A}_{12}\mathbb{B}_{11})q_i + \mathbb{B}_{11}^T\mathbf{p}_i = -\mathbb{A}_{12}F_i. \quad (26)$$

Adding the four equations in (26), and noting that the column-wise sums of  $\mathbb{B}_{11}^T$  are all zero (as the row-wise sums of the matrix  $\mathbb{B}_{11}$ , shown in (25), are all zero) eliminates the pressure unknowns, resulting in a single equation in only  $q_i^s$  for  $s \in \mathcal{C}$ . This, along with the mass conservation equations, determines the refined fluxes.

In Appendix A, we show the resulting equation is identical to the irrotationality equations (Equations (12) and (3)) determined in Section 2 in the case of zero recharge. Therefore, face-centered cells always have the same solution. In the node-centered cells with recharge, the difference is derived in the appendix. This difference is small for all calculated examples. Therefore, both mixed finite-element methods for the first-order equations and the discrete mass conservation equations (along with an irrotationality constraint) may be used to define a series of local problems for locally mass-conserving fluxes on a refined mesh. These fluxes are consistent with a given second-order-form pressure solution.

## 4. Numerical Examples

To illustrate the use of this method, we consider three examples. Each example is specified on the same domain,  $\Omega = [0, 1] \times [0, 1]$ , discretized on a regular Cartesian mesh. In the first two examples, an analytic pressure and permeability are specified. From these, analytic velocity and consistent forcing terms are calculated using Equations (1) and (2). This exact solution is then compared to computational tests, where the permeability and forcing are specified. Pressure solutions are calculated using bilinear finite elements (where the resulting linear systems are solved using the BoxMG multigrid package (*Dendy* [1982])), and velocities are calculated as in Sections 2 and 3.

For the final example, the permeability field is chosen to be a subdomain of that given within a single layer of the SPE 10 Benchmark problems (*Christie and Blunt* [2001]). Results are compared to finely-resolved calculations.

### 4.1. Smooth, Anisotropic Permeability

We first consider the case of a full-tensor permeability, whose entries are constant:

$$\mathcal{K} = \begin{bmatrix} 2 & 1 \\ 1 & 2 \end{bmatrix} \quad (27)$$

The analytic pressure solution is given by:

$$p(x, y) = y^2(1-y)^2x(1-x) + (1-x). \quad (28)$$

Solutions are run for varying grid resolutions, and convergence results are shown in Figure 7. Note that, as expected, pressure converges with second-order accuracy. While linear convergence is expected in the velocity solutions, the aggregated velocity on mesh-edge centers is superconvergent and

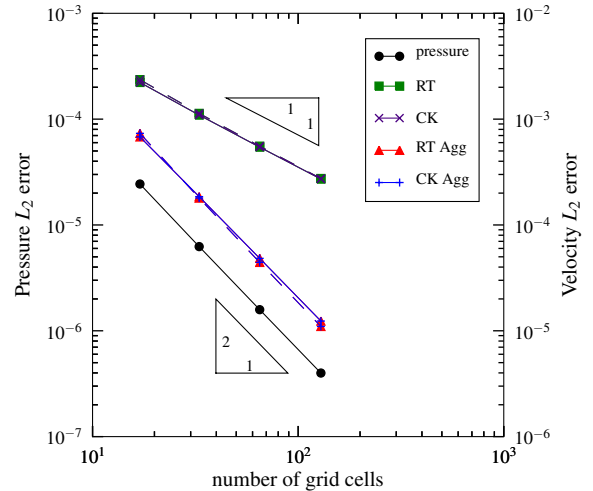


**Figure 7.** Convergence of the example in Section 4.1, a constant, full-tensor permeability field with polynomial pressure. At left, the accuracy of the pressure solution across grids. In the velocity convergence plot at right, solid lines are  $x$ -velocity while dashed are  $y$ -velocity (though the difference in errors is, in this case, not visible). Velocities calculated on the refined mesh using both the local-problem, Raviart-Thomas based method (RT) and the modified Cordes and Kinzelbach method (CK) are, as expected, first order. Aggregated fluxes (or average velocity), defined on the original pressure mesh super-converge with second-order accuracy at grid mid-points.

also second-order accurate. This problem has a non-zero source term, and mass conservation is exact by construction. Also, as both the recharge terms and permeability are smooth, the difference in errors is small – less than 0.1% of the total error in both the  $L_2$  and  $L_\infty$  norms.

#### 4.2. Interface Example

This example prescribes an interface at  $x = \frac{1}{2}$ , with the permeability on the left,  $\mathcal{K}_1 = 100$ , and on the right,  $\mathcal{K}_2 = 1$ .

$$p(x, y) = \begin{cases} 1 + 4x + xy^2 + 2x^2y^2 & 0 \leq x < \frac{1}{2}, \\ \beta_0 + 4\alpha x + \beta_1 xy^2 - \beta_2 x^2 y^2 & \frac{1}{2} \leq x \leq 1 \end{cases} \quad (29)$$

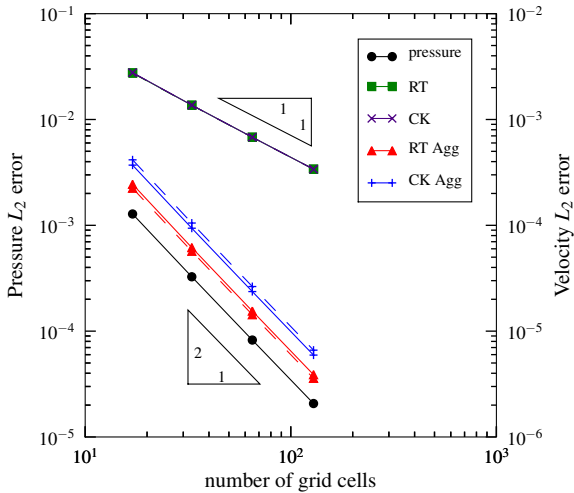


**Figure 8.** Convergence of the example in Section 4.2, an interface of two regions with constant permeability. Conventions are as in Figure 7. Here, however, recharge terms are irregular enough for the terms derived for the Raviart-Thomas local problems to become important, especially in the more accurate aggregate solution.

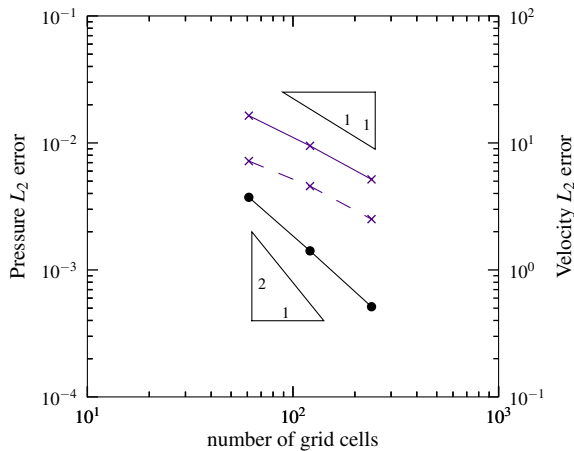


**Figure 9.** Convergence rates of pressure (dots) and velocities in two directions (crosses) of a series of problems on the permeability field in Figure 10. Note the piecewise-constant nature of the permeability affects the convergence rates in the  $L_2$  norm.

where

$$\begin{aligned} \alpha &= \frac{\mathcal{K}_1}{\mathcal{K}_2}, & \beta_1 &= 4 - 3\alpha, \\ \beta_0 &= 3 - 2\alpha, & \beta_2 &= 4 - 6\alpha, \end{aligned}$$

Boundary conditions are entirely Dirichlet, given by evaluating the above pressure field at the boundaries, but the problem directs flow in both  $x$  and  $y$  directions. Convergence rates are shown in Figure 8. Here, because of the variability in permeability and recharge, the difference between the methods derived in Appendix A is evident. The Raviart-Thomas local problem solutions are more accurate in both the un-aggregated ( $\sim 0.01\%$  more accurate in the  $L_2$  norm) and aggregated ( $\sim 30\%$  more accurate) cases, but the true advantage is in the aggregated cases, where more accurate treatment of source terms becomes non-negligible.

#### 4.3. Highly Discontinuous Permeability

Finally, we consider a section of the permeability provided for the SPE 10 Benchmark, taken from layer 70, which is well in the fluvial Upper-Ness permeability region of the benchmark. The permeability is scalar in the horizontal directions, but highly channelized and discontinuous in the section taken. Boundary conditions are applied as  $p(x = 0, y) = 1$  and  $p(x = 1, y) = 0$ , with no flux across  $y = 0, 1$ , and no source terms (indicating that the local problem equations and irrotationality equations are identical, and both methods provide the same fluxes). Convergence is tested on a series of problems, starting with the coarsest scale of  $61 \times 221$ , where each cell is a single permeability in the SPE model. These solutions are compared to a highly-resolved,  $481 \times 1761$  simulation. Convergence rates are shown in Figure 9, and the coarse-scale solution is shown in Figure 10.

## 5. Conclusions

We demonstrate two methods for post-processing second-order, GFEM pressure solutions for explicitly locally mass-conservative fluxes. Unlike most other post-processing techniques, which require the solution of a global problem on the entire domain, this method requires only the solution of local problems. This property makes it an ideal candidate for second-order upscaling algorithms, on which global problems are computationally infeasible. These approaches work by applying a control volume to the discretely enforced conservation principle enforced by the second-order weak form.

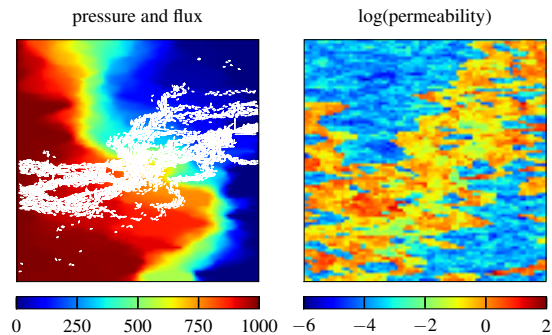


**Figure 10.** Pressure (with flux vector glyphs) and log of permeability for the solution of the SPE Benchmark 10 problem in Section 4.3, under flooding boundary conditions.

The two methods are demonstrated and compared on a series of analytic problems, and superconvergence on mesh edge centers is demonstrated. Finally, we present an example application of the method to a commonly used benchmark problem with physically realistic permeability fields.

**Acknowledgments.** This work was partially sponsored by the Department of Energy Computational Science Graduate Fellowship of the Office of Science and National Nuclear Security Administration under contract DE-FG02-97ER25308, and by the Department of Energy at Los Alamos National Laboratory under contracts DE-AC52-06NA25396 and the DOE Office of Science Advanced Computing Research (ASCR) program in Applied Mathematical Sciences. LA-UR 09-08292.

## Appendix A: Irrotationality and Equation (26)

The geometrically based irrotationality equations presented in Section 2 and the Raviart-Thomas system discussed in Section 3 provide two ways to define well-posed local problems for locally conservative fluxes. Here, we compute the difference between the two methods. To do this, we first calculate the closure equation in the Raviart-Thomas problem; this equation, along with three mass balance equations, determines the fluxes.

In Section 3.2, the Raviart-Thomas system on a dual-cell around a node is manipulated to arrive at a single closure equation for the undetermined set of mass balances. Specifically, block elimination led to the reduced system given in Equation (26), restated for convenience:

$$(\mathbb{A}_{11} + \mathbb{A}_{12}\mathbb{B}_{11})q_i + \mathbb{B}_{11}^T \mathbf{p}_i = -\mathbb{A}_{12}F_i. \quad (\text{A1})$$

The details of the closure equation are now derived for comparison by summing the rows of this reduced system. In the case of a diagonal tensor permeability on a uniform rectangular mesh, matrix  $\mathbb{A}_{11}$  is written as

$$\mathbb{A}_{11} = \begin{bmatrix} \gamma_{11}^{NE,NW} & \alpha^{NW} & 0 & \alpha^{NE} \\ \alpha^{NW} & \gamma_{22}^{NW,SW} & \alpha^{SW} & 0 \\ 0 & \alpha^{SW} & \gamma_{11}^{SW,SE} & \alpha^{SE} \\ \alpha^{NE} & 0 & \alpha^{SE} & \gamma_{22}^{SE,NE} \end{bmatrix}, \quad (\text{A2})$$

where

$$\begin{aligned} \alpha^e &= \frac{1}{12} \left( \frac{1}{\mathcal{K}_{11}^e} + \frac{1}{\mathcal{K}_{22}^e} \right) \\ \beta_k^{e1,e2} &= \frac{1}{6} \left( \frac{1}{\mathcal{K}_{kk}^{e1}} + \frac{1}{\mathcal{K}_{kk}^{e2}} \right) \\ \gamma_k^{e1,e2} &= \alpha^{e1} + \alpha^{e2} + \beta_k^{e1,e2}. \end{aligned}$$

The row and column ordering is  $\{q_i^N, q_i^W, q_i^S, q_i^E\}$ . Similarly, the matrix  $\mathbb{A}_{12}$  is written as

$$\mathbb{A}_{12} = \begin{bmatrix} \delta^{NW} & \delta^{NW} & 0 & 0 \\ 0 & -\delta^{SW} & -\delta^{SW} & 0 \\ 0 & 0 & \delta^{SE} & \delta^{SE} \\ -\delta^{NE} & 0 & 0 & -\delta^{NE} \end{bmatrix}, \quad (\text{A3})$$

where

$$\delta^e = \frac{1}{12} \left( \frac{1}{\mathcal{K}_{22}^e} - \frac{1}{\mathcal{K}_{11}^e} \right). \quad (\text{A4})$$

The columns of  $\mathbb{A}_{12}$  are indexed as  $\{Q_i^{NW}, Q_i^{SW}, Q_i^{SE}, Q_i^{NE}\}$ .  $\mathbb{B}_{11}$  is given in Equation (25).

Summing the four rows of (A1) results in

$$\begin{aligned} &3 \left( \beta_{11}^{NE,NW} q_i^N + \beta_{22}^{NW,SW} q_i^W + \beta_{11}^{SW,SE} q_i^S + \beta_{22}^{SE,NE} q_i^E \right) \\ &= 2 \left( \delta^{NW} F^{NW} - \delta^{SW} F^{SW} + \delta^{SE} F^{SE} - \delta^{NE} F^{NE} \right), \end{aligned} \quad (\text{A5})$$

where the pressure unknowns have been eliminated because the column sums of  $\mathbb{B}_{11}^T$  are zero. This closure of the Raviart-Thomas system is readily compared with the equivalent closure of the same mass balance equations in the modified Cordes and Kinzelbach approach, given in Equation (12). In the case of a diagonal permeability tensor, Equation (12) may be written as

$$\left( \beta_{11}^{NE,NW} q_i^N + \beta_{22}^{NW,SW} q_i^W + \beta_{11}^{SW,SE} q_i^S + \beta_{22}^{SE,NE} q_i^E \right) = 0. \quad (\text{A6})$$

Hence, the only difference between these closures is the forcing. Therefore, the difference between the solutions that results from these closures,  $\Delta q_i^s$  for  $s \in \mathcal{C}$ , is given by

$$\mathbb{C}\Delta q_i = \Delta \mathbb{F}_i, \quad (\text{A7})$$

where  $\Delta \mathbb{F}_i = [0, 0, 0, r]^T$ ,

$$r = \frac{2}{3} \left( \delta^{NW} F^{NW} - \delta^{SW} F^{SW} + \delta^{SE} F^{SE} - \delta^{NE} F^{NE} \right)$$

, and the matrix may be written as

$$\mathbb{C} = \begin{bmatrix} 1 & -1 & 0 & 0 \\ 0 & 1 & -1 & 0 \\ 0 & 0 & 1 & -1 \\ \beta_{11}^{NE,NW} & \beta_{22}^{NW,SW} & \beta_{11}^{SW,SE} & \beta_{22}^{SE,NE} \end{bmatrix}. \quad (\text{A8})$$

Given the structure of  $\Delta \mathbb{F}_i$ , it is apparent that the difference is captured completely by the fourth column of the inverse of  $\mathbb{C}$ . Inversion of  $\mathbb{C}$  then gives

$$\Delta q_i^s = r \left( \beta_{11}^{NE,NW} + \beta_{22}^{NW,SW} + \beta_{11}^{SW,SE} + \beta_{22}^{SE,NE} \right)^{-1} \quad (\text{A9})$$

for each  $s \in \mathcal{C}$ . Thus,  $r$  is a key scaling factor in the difference between these methods and, in many cases, it is small or zero. For example, in an isotropic medium, all  $\delta^e$ 's are zero and hence  $r = 0$ , and the two methods are identical. If the source term and permeability tensor are smooth functions, then Taylor expansion shows that cancellation eliminates the first-order terms. Moreover, even for smooth interfaces between highly anisotropic regions, cancellation on either side of the interface occurs, making  $r$  relatively small. The difference is largest when source terms and anisotropic permeability are highly variable on the scale of the grid spacing.

For element-centered dual cells, the two methods are identical. Specifically, the Raviart-Thomas equations have the same form as derived above for the node-centered case, but there is no source term in the element-centered dual cell.

## References

- Alcouffe, R. E., A. Brandt, J. E. Dendy, and J. W. Painter (1981), The multigrid method for the diffusion equation with strongly discontinuous coefficients, *SIAM J. Sci. Stat. Comput.*, 2, 430–454.
- Arbogast, T. (2000), Numerical subgrid upscaling of two-phase flow in porous media, in *Numerical treatment of multiphase flows in porous media (Beijing, 1999), Lecture Notes in Phys.*, vol. 552, pp. 35–49, Springer, Berlin.

- Carey, G., S. Chow, and M. Seager (1985), Approximate boundary-flux calculations, *Computer Methods in Applied Mechanics and Engineering*, 50(2), 107–120.
- Carey, G. F. (2002), Some further properties of the superconvergent flux projection, *Communications in Numerical Methods in Engineering*, 18(4), 241–250, doi:10.1002/cnm.483.
- Christie, M. A., and M. J. Blunt (2001), Tenth SPE comparative solution project: A comparison of upscaling techniques, *SPE Reservoir Evaluation & Engineering*, 4, 308–317.
- Cockburn, B., J. Gopalakrishnan, and H. Wang (2007), Locally conservative fluxes for the continuous Galerkin method, *SIAM J. Numer. Anal.*, 45(4), 1742–1776, doi:10.1137/060666305.
- Cordes, C., and W. Kinzelbach (1992), Continuous groundwater velocity fields and path lines in linear, bilinear and trilinear finite elements, *Water Resour. Res.*, 28(11), 2903–2911.
- Cordes, C., and W. Kinzelbach (1996), Application of the mixed hybrid finite element approximation in a groundwater flow model: Luxury or necessity? Comment, *Water Resour. Res.*, 32(6), 1905–1909.
- Dendy, J. E. (1982), Black box multigrid, *J. Comput. Phys.*, 48, 366–386.
- Efendiev, Y., and L. Durlofsky (2002), Numerical modeling of subgrid heterogeneity in two phase flow simulations, *Water Resour. Res.*, 38.
- Hou, T., and X. Wu (1997), A multiscale finite element method for elliptic problems in composite materials and porous media, *J. Comput. Phys.*, 134, 169–189.
- Hou, T., X. Wu, and Z. Cai (1999), Convergence of a multiscale finite element method for elliptic problems with rapidly oscillating coefficients, *Math. Comp.*, 68, 913–943.
- Hughes, T., G. Engel, L. Mazzei, and M. Larson (2000), The continuous Galerkin method is locally conservative, *J. Comput. Phys.*, 163(2), 467–488.
- Hughes, T. J. R., G. R. Feijóo, L. Mazzei, and J.-B. Quincy (1998), The variational multiscale method – a paradigm for computational mechanics, *Comput. Methods Appl. Mech. Engrg.*, 166, 3–24.
- MacLachlan, S. P., and J. D. Moulton (2006), Multilevel upscaling through variational coarsening, *Water Resour. Res.*, 42(2), doi:10.1029/2005WR003940.
- Mosé, R., P. Siegel, P. Ackerer, and G. Chavent (1994), Application of the mixed hybrid finite element approximation in a groundwater flow model: Luxury or necessity?, *Water Resour. Res.*, 30(11), 3001–3012.
- Raviart, P., and J. Thomas (1977), Primal hybrid finite-element methods for 2nd-order elliptic equations, *Mathematics of Computation*, 31(138), 391–413.
- Ruge, J. W., and K. Stüben (1987), Algebraic multigrid (AMG), in *Multigrid Methods, Frontiers in Applied Mathematics*, vol. 3, edited by S. F. McCormick, pp. 73–130, SIAM, Philadelphia, PA.
- Wheeler, M. F. (1974), A Galerkin procedure for estimating the flux for two-point boundary value problems, *SIAM J. Numer. Anal.*, 11, 764–768.

---

E. T. Coon, Applied Physics and Applied Mathematics, Columbia University, MC 4701, New York, NY, 10027, USA. (etc2103@columbia.edu)

S. P. MacLachlan, Department of Mathematics, Tufts University, Medford, MA, 02155, USA. (Scott.MacLachlan@tufts.edu)

J. D. Moulton, Mathematical Modeling and Analysis Group, Los Alamos National Laboratory, Los Alamos, NM 87545, USA. (moulton@lanl.gov)